

Misaligned streamers around a galactic centre black hole from a single cloud’s infall

W.E. Lucas^{1*}, I.A. Bonnell¹, M.B. Davies² & W.K.M. Rice³

¹ SUPA, School of Physics & Astronomy, University of St Andrews, North Haugh, St Andrews, Fife KY16 9SS, United Kingdom

² Lund Observatory, Department of Astronomy and Theoretical Physics, Box 43, SE-221 00 Lund, Sweden

³ SUPA, Institute for Astronomy, University of Edinburgh, Blackford Hill, Edinburgh EH9 3HJ, United Kingdom

24 March 2022

ABSTRACT

We follow the near radial infall of a prolate cloud onto a $4 \times 10^6 M_{\odot}$ supermassive black hole in the Galactic Centre using smoothed particle hydrodynamics (SPH). We show that a prolate cloud oriented perpendicular to its orbital plane naturally produces a spread in angular momenta in the gas which can translate into misaligned discs as is seen in the young stars orbiting Sagittarius A*. A turbulent or otherwise highly structured cloud is necessary to avoid cancelling too much angular momentum through shocks at closest approach. Our standard model of a $2 \times 10^4 M_{\odot}$ gas cloud brought about the formation of a disc within 0.3 pc from the black hole and a larger, misaligned streamer at 0.5 pc. A total of $1.5 \times 10^4 M_{\odot}$ of gas formed these structures. Our exploration of the simulation parameter space showed that when star formation occurred, it resulted in top-heavy IMFs with stars on eccentric orbits with semi-major axes 0.02 to 0.3 pc and inclinations following the gas discs and streamers. We suggest that the single event of an infalling prolate cloud can explain the occurrence of multiple misaligned discs of young stars.

Key words: Galaxy: centre – stars: formation – accretion, accretion discs – hydrodynamics

1 INTRODUCTION

Krabbe et al. (1991) first discovered twelve definite massive O and Wolf–Rayet (W–R) stars orbiting our Galaxy’s central black hole (BH) Sagittarius A* (Sgr A*). Krabbe et al. (1995) raised this to twenty-four, and more recently Bartko et al. (2010) counted 177. These stars are intriguing for their unusual situation. They appear to be coeval, having formed roughly 6 Myr ago (Paumard et al. 2006). All orbit at distances between roughly 0.05 and 0.5 pc of Sgr A*. Further astrometric and spectroscopic measurements have confirmed that these stars form at least one eccentric ($e = 0.36 \pm 0.06$) disc- or ring-like structure (Genzel et al. 1996; Genzel et al. 2003; Paumard et al. 2006; Lu et al. 2009; Bartko et al. 2009; Bartko et al. 2010) and fit a top-heavy IMF (eg. $dN \propto m^{-0.45 \pm 0.3} dm$, Bartko et al. 2010). Interestingly, a reasonable subset of the stars rotate oppositely in the plane of the sky. Paumard et al. (2006) and Bartko et al. (2009) concluded that these stars form a secondary stellar disc or streamer, although its existence is statistically less certain (Lu et al. 2009).

It seems likely that these stars were formed in a single event, though their unusual location and configuration complicate matters. Gerhard (2001) suggested that a massive cluster similar to Arches or the Quintuplet could infall to the BH via dynamical friction with the background stars. The remnant cluster core would be

deposited there. However, timescale arguments make this difficult (see Hansen & Milosavljević 2003 and the discussions in Alexander 2005 and Genzel, Eisenhauer & Gillessen 2010). Another scenario is that of the stars’ formation *in situ* within an accretion disc around the BH (Levin & Beloborodov 2003). While ‘normal’ star formation within a cloud so close to the BH would be strongly inhibited by tidal forces, a disc formed from such a cloud’s tidal shearing around the BH may become self-gravitating to such a degree that fragmentation may occur (Kolykhalov & Syunyaev 1980; Shlosman & Begelman 1989; Collin & Zahn 1999; Goodman 2003; Levin & Beloborodov 2003; Nayakshin & Cuadra 2005; Nayakshin, Cuadra & Springel 2007).

In agreement, numerical simulations have shown that portions of an infalling cloud can be captured by a BH to form an eccentric disc that fragments to form a stellar disc population (Bonnell & Rice 2008; Hobbs & Nayakshin 2009; Alig et al. 2011; Mapelli et al. 2012). Bonnell & Rice (2008) found that heating of the gas as it was compressed around the BH raised the Jeans mass, leading to the formation of a population of high mass stars in inner regions around the BH. Lower mass stars formed farther out in a separate population. Hobbs & Nayakshin (2009) found that a collision between two clouds close to Sgr A* could be responsible for the formation of multiple discs, though this would require two clouds to simultaneously enter the innermost Galactic Centre (GC). Two populations of stars formed in the same manner as in Bonnell & Rice (2008).

* E-mail: wel2@st-andrews.ac.uk

In this paper we use smoothed particle hydrodynamics to examine a model similar to that of Bonnell & Rice (2008), requiring only one cloud on infall towards a BH – a simpler and perhaps more frequent event. The cloud’s geometry is prolate to the orbital plane, generating a large spread in angular momentum when on a highly radial orbit as gas flows around the BH from different directions. This naturally leads to the formation of multiple misaligned gas structures orbiting the central BH.

2 NUMERICAL METHOD

2.1 Smoothed particle hydrodynamics

Smoothed particle hydrodynamics (SPH) is a Lagrangian hydrodynamics formalism in which particles are used to represent portions of the total gas mass. A good description of the formalism is provided by Monaghan (1992). We used the code of Bate, Bonnell & Price (1995), itself derived from an earlier SPH code (Benz 1990; Benz et al. 1990). This code includes individual particle timesteps (eg. Hernquist & Katz 1989) and is parallelized using OpenMP. Sink particles, which are the SPH representations of (proto-)stars, were implemented following Bate et al. (1995).

Radiative transfer of energy was approximated with the hybrid method of Forgan et al. (2009). Standard SPH shock heating and $p dV$ work were combined with the polytropic cooling technique of Stamatellos et al. (2007) and the flux-limited diffusion method of Mayer et al. (2007). Polytropic cooling alone was used by Bonnell & Rice (2008) and allowed energy transfer with an external radiation background. This took the form of cooling when the gas had a higher temperature than the background, and heating when it was lower. The radiative diffusion used here further improved the approximation by allowing energy to flow from hot to cold gas, the flux-limiter regulating the flow appropriately between the optically thick and thin limits. We used a background temperature of $T_{\text{bg}} = 100$ K, close to the values observed in GC molecular and atomic gas (Jackson et al. 1993; Martín-Pintado et al. 1997; Christopher et al. 2005). Once a particle’s time derivative of the internal energy had been calculated, it was semi-implicitly integrated as described by Forgan et al. (2009), following Stamatellos et al. (2007). In contrast to both this work and Bonnell & Rice (2008), the cooling of Hobbs & Nayakshin (2009) was determined via a parametric relation with the dynamical timescale.

Particles were integrated in thirty timestep bins, each with a power of two division of the maximum timestep $\Delta t_{\text{max}} = 236$ yrs, or 5×10^{-4} in code units (one code unit was equivalent to 1.4874×10^{13} s). The smallest timestep a particle could be integrated on was $\Delta t_{\text{max}}/2^{29} = 14$ s, though typically few ever required a timestep shorter than $\Delta t_{\text{max}}/2^{20} = 2$ hours. While a large BH accretion radius (see Section 2.2) delayed it, the accretion to the disc of cloud material over time eventually caused particle timesteps to fall below the minimum, ending the simulation. To keep the simulation running would have required reducing the maximum timestep or increasing the number of bins: either would have unreasonably increased the integration time.

Gas in the simulation experienced the potential from the nuclear stellar cluster in addition to the BH and its own self-gravity. To obtain the enclosed mass as a function of Galactocentric radius R , we integrated over volume the stellar number density of Merritt (2010), who constructed a model using observations by Schödel et al. (2007) and Buchholz, Schödel & Eckart (2009). This number

density is given as

$$n(R) = n_0 \left(\frac{R}{R_0} \right)^{-\gamma_i} \left[1 + \left(\frac{R}{R_0} \right)^\alpha \right]^{(\gamma_i - \gamma)/\alpha}. \quad (1)$$

To tabulate the masses we used their best fit parameters of $\gamma_i = -1.0$, $\gamma = 1.8$ and $\alpha = 4.0$, $R_0 = 0.21$ pc, and normalized with the observed enclosed mass at $R = 1$ pc of $\approx 1 \times 10^6 M_\odot$ (Schödel, Merritt & Eckart 2009).

2.2 Sinks in SPH

Sinks are N-body particles that only experience gravitational forces, but can accrete nearby gas particles. Dynamic sink creation was used to model star formation. Following Bate et al. (1995), sinks were created to replace a bound, collapsing region of gas. Such a region was required to be smaller than the accretion radius of the sink which would replace it (see next paragraph), 10^{-3} pc. It was also required to exceed a critical density. In those runs which used clouds with masses $10^4 M_\odot$ and $2 \times 10^4 M_\odot$, it was $10^{-11} \text{ g cm}^{-3}$, while for the clouds of $10^5 M_\odot$, which were less dense initially, it was $6.4 \times 10^{-12} \text{ g cm}^{-3}$. These are of order ten million times the initial cloud densities. They also approximate the tidal density at the BH’s outer accretion radius, helping prevent sink formation where tidal disruption is likely. Once a region fulfilling the above requirements was identified, further checks were made to ensure that the region was both bound and collapsing, as described by Bate et al. (1995). The initial mass for sink particles was approximately fifty times the gas particle mass. For clouds with $2 \times 10^4 M_\odot$, this was $0.3 M_\odot$; for $10^5 M_\odot$, it was $1.5 M_\odot$. Taken together, these tests ensured that a real and resolved star formation event was taking place.

Accretion to a sink from within an outer accretion radius $r_{\text{acc,out}}$ was only allowed if the gas was bound to the sink, and more tightly than to any other sink, and if its angular momentum around it was small enough to allow it to enter a circular orbit at $r_{\text{acc,out}}$. Conversely, all gas was accreted once it fell within an inner accretion radius $r_{\text{acc,in}}$. We used $2.5 \times 10^{-4} \text{ pc} \approx 50 \text{ AU}$ for both the stars and the BH. $r_{\text{acc,out}} = 10^{-3} \text{ pc} \approx 200 \text{ AU}$ was used for sink particles representing stars, the same as the critical sink creation radius. The outer accretion radius was chosen to approximate the size of a protostellar disc; therefore a sink particle may be taken to represent an unresolved star-disc system. This radius was chosen as an acceptable tradeoff between simulation runtime, decreased with increasing r_{acc} , and sink resolution, improved with decreased r_{acc} .

We represented the black hole with a sink particle of mass $4 \times 10^6 M_\odot$ (Ghez et al. 2008). In order to avoid relativistic effects and huge forces on gas particles, we increased its outer accretion radius to 0.02 pc. At this distance from the BH, the Keplerian circular speed was 0.3 per cent of the speed of light. The inner accretion radius was the same as that used for dynamically created sinks.

It is important to note that dynamically-created sink particles do not represent true stars. Rather, they consist of an unresolved accretion disc and (proto)star that exist within the accretion radius. Likewise, the large accretion disc around the BH would in reality extend inside the outer accretion radius.

2.3 Physical setup

The simulations followed the infall of a single prolate ellipsoidal cloud. The parameters for each are listed in Table 1. The cloud had had semi-minor axis r and semi-major axis h , and was positioned

Table 1. Run names and their initial conditions. M_{cl} was the cloud’s mass, r was the length of its semi-minor axis and h its semi-major axis. The cloud was given an initial velocity \mathbf{v}_{cl} ; integrating the system by replacing the cloud with a point mass gave the minimum distance from the BH R_{min} during the pass. Other changes are noted. t_{end} is the final simulation time. ΔM_{BH} is the mass accreted to the BH during the simulation. Finally we have the number of sinks formed by the run’s end N_{sink} and the total mass in sinks $M_{\text{sink,tot}}$ (excluding the BH). Note these values are not directly comparable as the simulations finished at different times.

Run name	M_{cl}/M_{\odot}	$r(\text{pc})$	$h(\text{pc})$	$\mathbf{v}_{\text{cl}}(\text{km s}^{-1})$	$R_{\text{min}}(\text{pc})$	Notes	$t_{\text{end}}(\text{yrs})$	$\Delta M_{\text{BH}}(M_{\odot})$	N_{sink}	$M_{\text{sink,tot}}(M_{\odot})$
A	2×10^4	0.4	1.0	(−41.5, 10.4, 0)	0.022	-	28300	1280	14	21.9
A re-run	2×10^4	0.4	1.0	(−41.5, 10.4, 0)	0.022	-	30890	4290	10	9.00
B	2×10^4	0.4	1.0	(−41.5, 10.4, 0)	0.028	No cluster	32540	553	19	32.0
C	2×10^4	0.4	1.0	(−41.5, 10.4, 0)	0.022	10^7 particles	26650	3870	5	3.93
D	1×10^4	0.4	1.0	(−41.5, 20.7, 0)	0.064	-	37020	45.8	25	59.2
E	1×10^4	0.4	1.0	(−41.5, 41.5, 0)	0.163	-	36650	0.00	109	375
F	1×10^5	1.0	2.5	(−41.5, 10.4, 0)	0.022	-	25000	8940	64	741
G	2×10^4	0.4	1.0	(−41.5, 10.4, 0)	0.022	Alt. turbulence	23110	726	17	62.6
H5	1×10^4	0.4	1.0	(−150, 5, 0)	0.006	-	15800	5230	1	1.95
H10	1×10^4	0.4	1.0	(−150, 10, 0)	0.021	-	15560	2830	0	0.00
H20	1×10^4	0.4	1.0	(−150, 20, 0)	0.060	-	16740	348	0	0.00
H40	1×10^4	0.4	1.0	(−150, 40, 0)	0.153	-	96220	5.59	0	0.00
I5	1×10^5	1.0	2.5	(−150, 5, 0)	0.006	-	25470	38200	1	1.59
I10	1×10^5	1.0	2.5	(−150, 10, 0)	0.020	-	27360	37100	0	0.00
I20	1×10^5	1.0	2.5	(−150, 20, 0)	0.060	-	18870	20000	68	1190
I40	1×10^5	1.0	2.5	(−150, 40, 0)	0.152	-	20750	2410	10	453

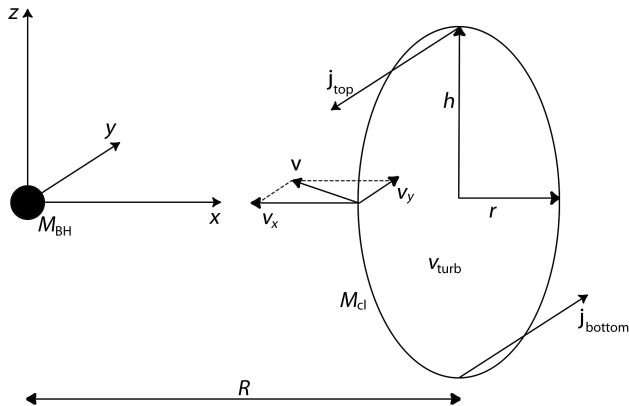


Figure 1. Here we show the initial simulation geometry, comprising two objects: a gas cloud of mass M_{cl} and a black hole (BH), represented by a sink particle of mass M_{BH} . The cloud was positioned such that its centre lay on the x -axis at a distance R from the BH which lay at the origin. It had a semi-minor axis of length r and semi-major axis of length h , which was aligned with the z -axis. The cloud was given an initial velocity \mathbf{v} which lay in the xy -plane, giving it an infall velocity v_x and a tangential velocity v_y . This ensures that specific angular momentum \mathbf{j} is spread over a large angle between particles at the top \mathbf{j}_{top} and bottom $\mathbf{j}_{\text{bottom}}$ of the cloud.

such that its centre lay at a distance $R = 3 \text{ pc}$ from the BH which was placed at the origin. Its major axis was parallel to the z -axis, while it was given an initial velocity \mathbf{v} in the xy -plane. The combination of the cloud’s shape and its highly radial orbit bestowed a large spread in angular momentum. The simplicity of this setup, depicted in Figure 1, is its principle attractive feature.

We also applied to the cloud an initial turbulent velocity field which provided support against its self-gravity and also generated structure – this proved to be crucial in the retention of the gas’s angular momentum about the BH, and will be discussed later in Section 3.2. The method used was that described by Dubinski et al. (1995) and Dobbs et al. (2005). The velocity field was drawn from

a power spectrum

$$P(k) \equiv \langle |v_k|^2 \rangle \propto k^{-n} \quad (2)$$

with $n = 3.5$, by randomly sampling a vector potential, making the field initially divergenceless. Gas particles velocities were interpolated from the output grid, and then scaled in all our simulations to give a ratio of turbulent kinetic to gravitational energies $|E_{\text{kin}}/E_{\text{grav}}| = 1.5$

The initial conditions of our simulations are shown in Table 1. The simulation we call Run A is used to demonstrate the model. It used $M_{\text{cl}} = 2 \times 10^4 M_{\odot}$, $r = 0.4 \text{ pc}$, $h = 1.0 \text{ pc}$ and $\mathbf{v}_{\text{cl}} = (-41.5, 10.4, 0) \text{ km s}^{-1}$. We used 3141792 particles to represent the gas.

We motivate our infall velocities from observations (Tsuboi et al. 2011) which have found little gas with line-of-sight speeds beyond 75 km s^{-1} within $\sim 35 \text{ pc}$ projected distance from the GC. Thus we initially used a low infall velocity of $v_x = -41.5 \text{ km s}^{-1}$. Calculations of infall from rest between 5 and 20 pc indicated that by $R = 3 \text{ pc}$, a test particle would be moving between 100 and 200 km s^{-1} due to the BH and cluster. As a result, we performed several more simulations using $v_x = -150 \text{ km s}^{-1}$.

Here we briefly discuss Run B and C as they were performed as tests of the setup. Run B did not include the stellar cluster. As expected, the missing extended potential caused the gas particles to follow trajectories more similar to closed Keplerian orbits than those in Run A. Otherwise they were very similar, demonstrating the dominance of the BH potential in the central parsec.

Run C was a resolution test, performed using 10 million particles. In order to ensure it ran long enough over a timescale similar to the other simulations, we relaxed the BH accretion rules, allowing it to accrete all gas within 0.02 pc without test. Although this only affected the innermost regions of the simulation, of secondary interest to the large scale gas dynamics, we re-ran Run A with the same accretion rules to allow a direct comparison. Run C’s improved mass resolution of $1.91 \times 10^{-3} M_{\odot}$ caused sinks to form at masses roughly three times smaller than in the other simulations. Despite this, by the time of comparison five sinks had formed and accreted to masses of $\approx 1 M_{\odot}$ in both simulations. The gas dis-

tribution was also highly comparable, with the only change being slightly higher densities close to the BH accretion radius. Consequently, the BH had accreted slightly more in Run C at $3870M_{\odot}$ compared to $3550M_{\odot}$ in the re-run of A. As such we accept the set of lower resolution simulations as being reasonably well resolved. We have included the re-run of A in Table 1, but do not discuss it further.

3 GAS DYNAMICS

3.1 Formation of a misaligned streamer

Run A provides a good demonstration of the sequence of events during infall and the formation of a misaligned structure. The cloud began its infall with uniform density, but the turbulence quickly generated structure and removed the symmetry between top and bottom. As the cloud drew closer, the tidal forces from the black hole began to pull the cloud apart. The tangential velocity given to the cloud was enough that its centre of mass passed to the side of the BH, giving enough angular momentum to prevent the majority of the cloud from being accreted.

During its pass of the BH, the cloud was tidally sheared, some of its mass being captured and forming a disc on the scale of ~ 0.1 pc. Compression of the gas as it flowed around the BH heated it to a maximum of 6000 K, before it expanded and was allowed to cool again. At closest approach, gas passed over and under the BH, which, combined with the tangential motions, produced streamers of gas with very different angular momenta. Gas which had accumulated in a central overdensity formed a small dense disc due to its comparatively low angular momentum. Another overdensity which had formed in the bottom (negative z region) of the cloud swept up to form a large streamer at 60° to the dense inner disc. By the end of the simulation, at $t = 28300$ yrs, $15500M_{\odot}$ of gas was bound within a distance of 1 pc from the BH, which had itself accreted $1280M_{\odot}$. Star formation in the cloud and disc produced 14 sinks (see Section 4). The process of infall can be seen in Figure 2.

Our decision to use a cloud prolate to the orbital plane was responsible for the creation of the misaligned gas streamer. Visualising the spread in angular momentum direction on the sky reveals the presence of the disc and streamer – Figure 3, shows this in two plots, for gas with semi-major axis less and greater than 0.7 pc. There are two peaks in the density of particles’ angular momentum orientations on the sky representing both the central disc and the streamer. The density is noticeably highest in the region inhabited by the disc for that gas on small orbits. In the second plot for gas on larger orbits, higher densities occur for the streamer. The overall distribution is visibly asymmetric about the $\theta = 0^{\circ}$ line – this asymmetry was present in the initial distribution. As discussed in Section 3.2, a more symmetric distribution results in the destruction of the misaligned streamers.

The asymmetry can also be seen in Figure 4 where gas at the end of Run A has been binned by each component of its specific angular momentum. While the mass distribution of the x -component l_x is symmetric, and that of l_z is offset due to the cloud’s non-zero initial v_y , the l_y distribution peaks at small negative values. This is the material originally within the top half of the cloud, much of which goes on to form the disc. The distribution then increases slowly to the l_y , forming a long but shallow tail of $\sim 2000M_{\odot}$. The gas in the streamer is found in this tail.

The streamer mass may be further constrained by binning the

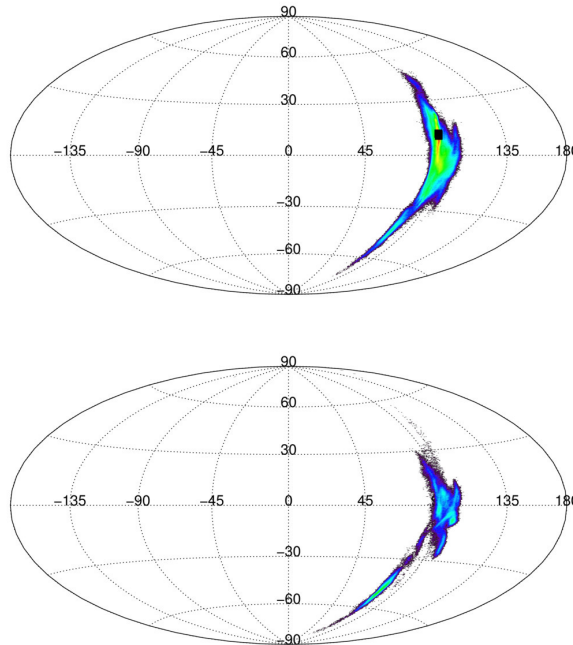


Figure 3. Angular momentum orientations on the sky for the gas particles in Run A at the run’s end at $t = 28300$ yrs in a Hammer projection. The first and second plot respectively show gas with semi-major axis less than and greater than 0.7 pc. The vectors’ components were calculated in (θ, ϕ) polar and azimuthal angles. These have been rotated such that the direction given by $(0, 90)^{\circ}$ points in positive z (see Figure 1) and corresponds to anticlockwise rotation in the xy -plane when looking down the z -axis. The direction $(0, 0)^{\circ}$ points along the x -axis, and $(-90, 0)^{\circ}$ along y . Particles were then placed in equal-area bins. The log of the number of particles in each bin has been plotted proportional to its shade, with both plots using the same colour scale. The large overall spread in angular momentum is apparent in both plots. The disc and streamer are seen as peaks in both plots located at $(10, 90)^{\circ}$ and $(-50, 75)^{\circ}$, separated by 60° . In the first plot the highest densities are located at the disc orientation. The black squares, representing sink particles, align very well with one another and the disc. For semi-major axes greater than 0.7 pc the disc and streamer are much more distinct, and the highest densities occur in the region of the streamer orientation.

gas by the angle between the y -axis and its angular momentum vector projected into the yz -plane, $\theta = \tan(l_z/l_y)$. This reveals a twin peaked distribution, as shown in Figure 5. The smaller peak, representing the misaligned gas, was located 60° away from the larger peak, which is the disc, and contained $1070M_{\odot}$. Only $560M_{\odot}$ of this orbited within 1 pc of the BH, the remainder on orbits with semi-major axes of up to 10 pc.

3.2 Importance of asymmetries

It is important for the infalling cloud to be structured if misaligned streamers are to form. If this is the case, the gas streams passing on either side of the BH do not shock completely and cancel their respective angular momenta. The turbulence used in Run A (see Figure 2) created sufficient structure to accomplish this.

To explore the importance of a particular turbulent velocity field, we performed Run G which can be seen in Figure 6. The alternative realisation failed to produce significant asymmetries. Thus, self-shocking of the flows occurred on reaching the BH. A disc

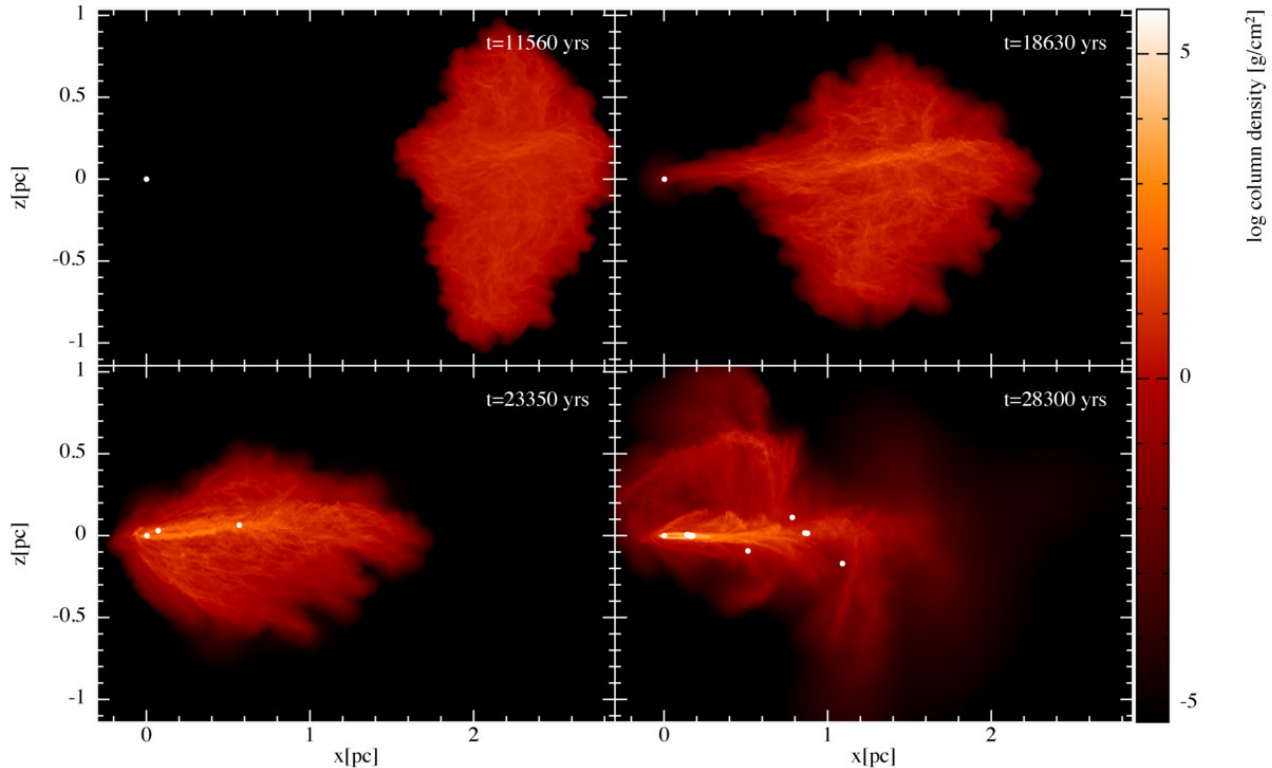


Figure 2. Column density in xz of Run A’s cloud at four times. The turbulence in the cloud generated enough structure that by the time it reached the black hole the flow around it was highly asymmetric, and had actually formed several sink particles. These though were on almost radial orbits and had semi-major axes of between 1 and 3 pc. The BH and dynamically created sink particles are shown as white dots. As a sink, the BH was allowed to move, and so was accelerated towards the cloud. However, its huge mass meant its motion is not visible on the scales shown here. The misaligned streamer can be seen to sweep up from below around the BH. It was however never dense enough to form sinks.

formed from the central regions, but the mirrored flows from the top and bottom met and shocked with one another. The disc itself was very small, with a radius ≈ 0.05 pc, and circular, again as a result of angular momentum cancellation.

A comparison between the total angular momentum at two times, including that of gas accreted to the BH, is telling. Between the start and the end of Run G, 20 per cent of the total angular momentum magnitude was cancelled out. Over the same period, 12 per cent of the angular momentum in Run A was cancelled out. A re-run of G using relaxed BH accretion rules progressed slightly further to 24050 yrs and experienced a further 7 per cent decrease. The plot of angular momentum distribution on the sky (Figure 7) shows symmetry above and below the equator which indicates roughly equal gas flows orbiting in opposite directions around the BH. Calculations show that there is a $70M_{\odot}$ difference in the mass of gas flowing in each direction in Run G, while in Run A at the same time the difference was $1205M_{\odot}$.

It is clear that for multiple structures to form, the various regions of the cloud which are to orbit the BH in such different planes must be able to retain their angular momentum, and it is self-shocking of the gas that acts to oppose to this. However, our use of turbulence was mainly to drive structure formation. Real molecular clouds are observed to be clumpy which would likely provide the asymmetry we require here.

3.3 Varying the cloud orbit

In other runs we varied the cloud’s initial velocity \mathbf{v} in order to examine the effect this had on the formation of the disc and any streamers. Run A used $v_x = -41.5 \text{ km s}^{-1}$ and a tangential speed of $v_y = 10.4 \text{ km s}^{-1}$. As such the cloud marginally engulfed the BH, though the majority of gas passed to one side.

Runs D and E used higher tangential speeds of $v_y = 20.7 \text{ km s}^{-1}$ and 41.5 km s^{-1} . The large v_y meant that the cloud’s trajectory in Run D missed the BH; very little gas was captured to form a disc. With the high v_y , the large spread in angular momentum bestowed by the cloud’s shape was compressed and the tidal arc formed during the pass around the BH was close to planar. The high angular momentum also meant that only small amounts of gas had been able to accrete onto the BH. The situation in Run E was even more extreme, as there was no disc formation or BH accretion. To form a single disc requires the cloud to move on an orbit that passes close enough to the BH that the cloud be tidally disrupted by it. From these two runs it is also apparent that for our cloud’s geometry to allow the formation of multiple structures the orbit must be radial to the point that the cloud passes within a distance from the BH less than its own semi-major axis h .

Alternatively, it may be stated that the angle from the BH between the cloud’s midplane and one of its tips, when at closest approach to the BH, is the maximum possible misalignment. Thus a head-on collision would produce a misalignment of 90° (although if the flows were symmetric, the angular momentum would be cancelled and the streamers would not form), while a distant

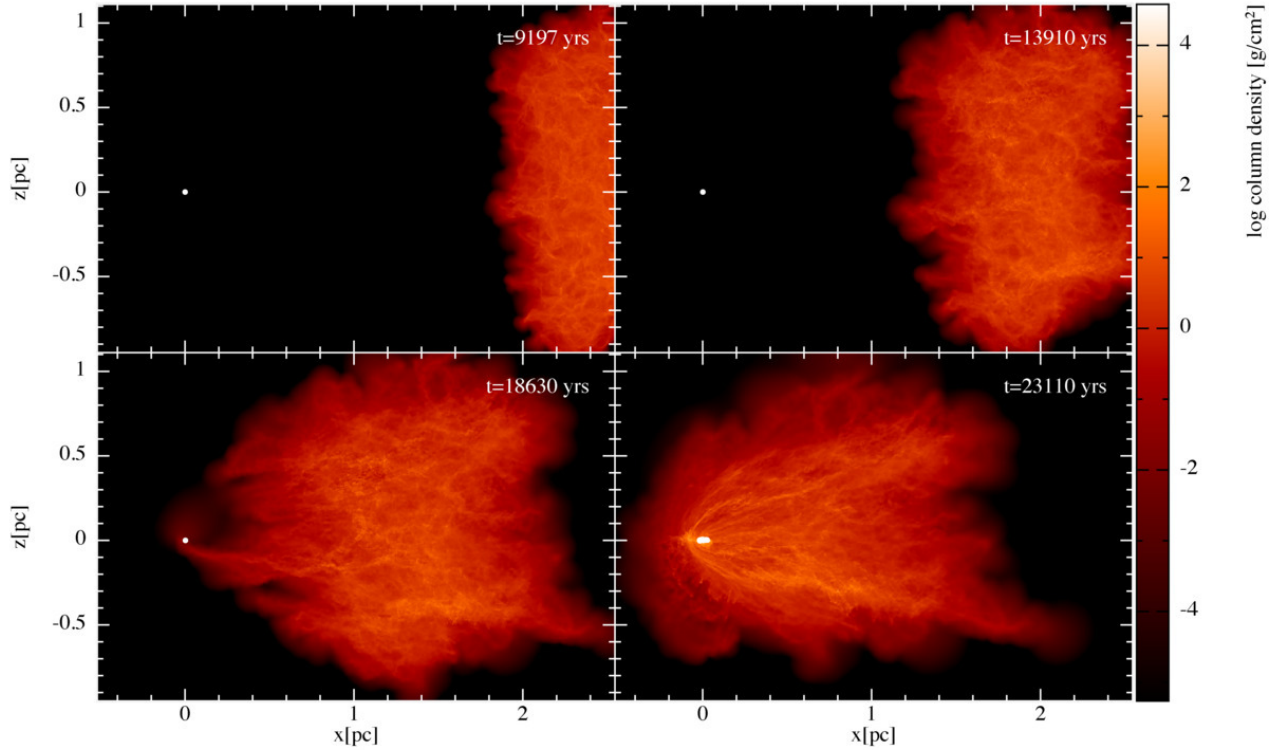


Figure 6. Column densities in the xz -plane throughout Run G. The initial state was exactly the same as that in Run A save that the turbulent velocity field was produced using different seed integers. This gave rise to a cloud lacking large overdense regions, and which was comparatively symmetric above and below the xy -plane. As can be seen, this led to the flows from these regions roughly mirroring one another and shocking on the other side of the BH. No misaligned structures formed. The cancellation of angular momentum via shocking also reduced the disc’s size and eccentricity.

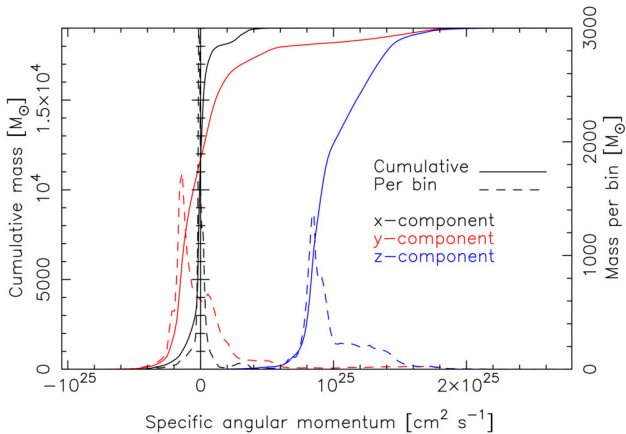


Figure 4. At $t = 28300$ yrs in Run A, the specific angular momentum for each gas particle around the BH was calculated. The particles were binned by each component of the angular momentum; here we show the cumulative mass across these bins, as well as the individual values. The black line, showing the x -component l_x , is comparatively symmetric about 0 as x was the infall axis. On the other hand, no gas has negative l_z . This is due to the initial tangential speed v_y given to the cloud, which gave rotation around the z -axis and thus positive angular momentum. The most interesting is the y -component. Most mass has negative values, with the peak in bin mass also seen at negative angular momentum. This is the disc, which formed from an overdensity slightly above the xy -plane and so possessed rotation around the y -axis. Gas misaligned with the disc, including the streamer, forms that part of the distribution extending to large positive l_y . It contains $\sim 2 \times 10^3 M_\odot$.

pass would form a single disc only, and then only if tidal forces were still able to disrupt it. That such nearly radial orbits are required may be the largest caveat to the formation of multiple stellar discs by this method.

The H and I runs all used the much higher infall speed $v_x = -150 \text{ km s}^{-1}$ predicted by the BH and cluster potential model. Each run’s name includes a number, 5, 10, 20, or 40, indicating the tangential speed v_y in km s^{-1} . While the H-runs used $M_{c1} = 10^4 M_\odot$, the clouds in the the I-runs had $10^5 M_\odot$ and axes twice as long as those of Run A’s cloud. This meant the I-runs’ clouds engulfed the BH even with $v_y = 40 \text{ km s}^{-1}$. Column density and angular momentum density plots are shown for these two sets of runs in Figures 8 and 9.

With the same turbulent velocities, these clouds formed the same overdensity in the cloud centre as in Run A from which it formed the disc. Positioned above the cloud’s midplane, with low v_y the disc formed not in the orbital xy -plane but almost in the xz -plane. As the tangential velocity v_y was increased, the disc rotated towards the xy -plane, clearly visible in Figures 8 and 9. This was reflected by the angular spread of angular momentum consolidating towards the z -axis with increasing v_y .

Infall was however so fast during these runs that asymmetries could not grow significantly, and shocking took place on the BH’s far side. No misaligned streamers such as those described in the previous section could form, except in the case Run I10. Gas from the top half of the cloud was able to pass downwards on its orbit and avoided shocking. As it reached the BH it was sheared further to form a disc on the scale $\approx 0.2 \text{ pc}$. This had not however depleted

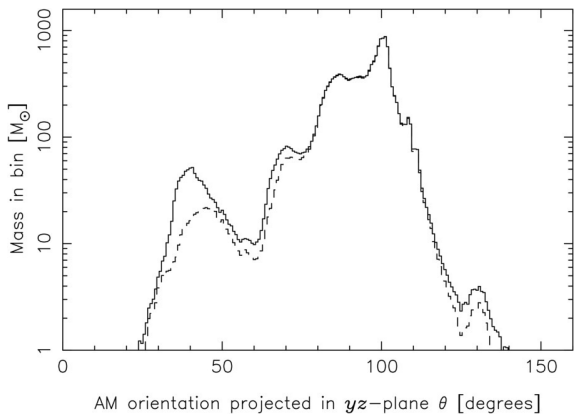


Figure 5. Here we show the gas in Run A at $t = 28300$ yrs, binned by the angle between the angular momentum vector projected into the yz -plane and the y -axis, given by $\theta = \tan(l_z/l_y)$. The solid line represents all gas in the simulation, while the dashed line shows only that which was bound to within one parsec; we have also given the bin values in logspace to better show the gas orbiting in planes misaligned with the disc. The disc makes up the large peak centred at 100° . At 40° a smaller peak can be seen, making up the streamer. In contrast with the disc, half the gas in the streamer is bound to within one parsec. If we define the streamer as containing all the gas with $\theta \leq 60^\circ$, then its total mass is $1070M_\odot$. The bound mass is $560M_\odot$. Of the remaining $17650M_\odot$, $17050M_\odot$ is bound.

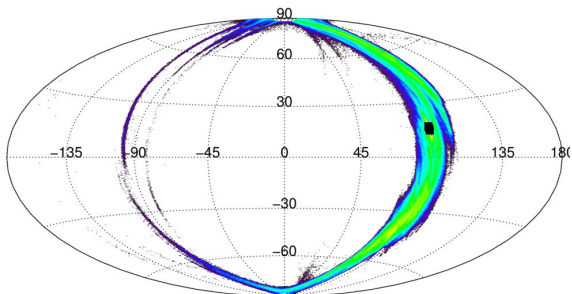


Figure 7. Density of angular momentum orientation in the sky for Run G at 23100 yrs, constructed in the same way as in Figure 3, though here we include all the gas. The disc is present as the densest region, aligned with the black squares representing the direction of the sinks' angular momentum. In comparison to Figure 3, this distribution for gas is roughly symmetric above and below the $\theta = 0^\circ$ line, representing a large spread in the angular momentum of the infalling gas. The gas lying above the equator has total mass $9540M_\odot$, while the counterrotating gas in the bottom hemisphere has a very similar $9610M_\odot$. At the same time, Run A had values of $10420M_\odot$ and $9215M_\odot$, a difference of more than a thousand solar masses. With the initial turbulent velocity field failing to generate significant structure, the misaligned gas flows met and shocked on the simulation xy -plane, preventing the formation of a streamer.

the gas reservoir, which still possessed a large range in angular momentum. Hence, as a different subset of the gas fell inwards and was itself sheared, it formed a second structure of similar density to the inner disc, but positioned slightly outside and oriented 17° out of plane.

The mass in gas that orbits close to the BH is an upper limit to the mass of any stellar disc. Figure 10 shows the time evolution of the mass in gas particles bound to within 1 pc and the mass accreted to the BH for all of the I-runs. (We remind the reader that

the BH sink particle represents not only the physical BH but also its unresolved inner accretion disc.) While the simulations end at different times, there is a clear trend of decreasing total mass (solid lines) with increasing initial cloud tangential velocity v_y . It is in accreted mass (long dashes) that the majority of the decrease occurs; the final mass accreted to the BH sink varied from almost $4 \times 10^4 M_\odot$ for I5 and I10, to only a few thousand M_\odot for I40. When v_y was low, the z -component of the angular momentum was reduced. Thus once shocking had taken place on the far side, itself enhanced by the high infall speed, very little angular momentum remained. Changes in the mass of bound gas (short dashes) are much smaller and indicate final values of 2 to $3 \times 10^4 M_\odot$ for these four runs. As such, with low v_y (Runs I5 and I10) the shocking was so effective at cancelling out angular momentum that more mass was accreted to the BH than remained bound in the gas phase. For Runs I20 and I40, this had reversed with more being bound and less accreted.

Only particles within 0.02 pc of the sink particle representing the BH could be accreted. Furthermore, they were required to have a low enough angular momentum to form a circular orbit at that radius. Assuming a particle's angular momentum remains constant during infall, its circularisation radius is $R_{\text{circ}} \propto l^2$ where l is the specific angular momentum. The low angular momentum needed to circularize within the BH's accretion radius was available to fewer particles when the cloud's initial v_y was higher. Meanwhile, those with larger angular momentum were still able to circularize within 1 pc.

4 STAR FORMATION

Although the focus of this paper is placed on the gas dynamics of a cloud infalling towards a massive BH, we here take time to discuss the star formation we observed in our simulations.

4.1 Star formation physics

We included an approximation of radiative cooling via the method of Forgan et al. (2009). Before fragmentation could even begin to occur, the gas disc had to become cool enough that thermal pressure would not impede collapse. This is normally described by the Toomre Q-criterion which also ensures that rotational energy cannot form a barrier against self-gravity.

A fragment's ability to collapse and form a star is dependent on the ability of the gas to cool quickly (Gammie 2001; Rice et al. 2003). As the parcel of gas contracts, it heats up, which would halt the collapse due to the increase of thermal pressure. If the gas can cool quickly, this should not be a problem and the collapse can continue. On the other hand if the cooling is slow the shear in the disc will disperse the fragment before it can collapse. This means that the cooling timescale must be shorter than a few times the disc's rotational period (Gammie 2001). In discs around SMBHs the cooling time is typically very short inside $R = 0.1$ pc (Levin & Beloborodov 2003; Levin 2007; Nayakshin et al. 2007; Alexander et al. 2008).

4.2 Sinks in the simulations

It was not uncommon for sinks to form in the cloud during slow infall ($v_y = -41.5 \text{ km s}^{-1}$). These were either unbound or on orbits with eccentricities approaching unity. Our interest however lay with star formation within a disc or streamer, as demonstrated in

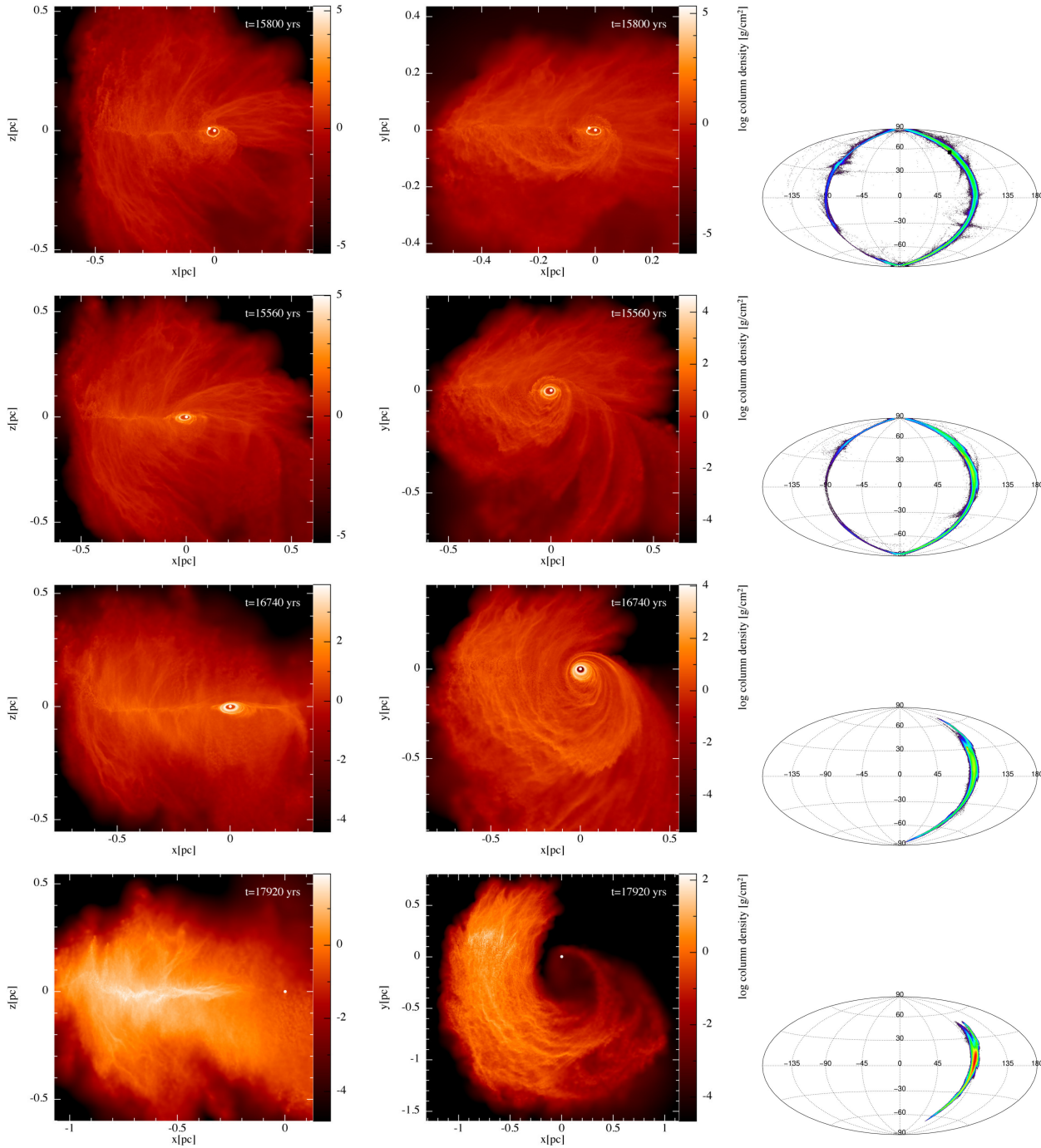


Figure 8. xz and xy column densities, and angular momentum spread of all gas in Hammer projection (see Figure 3) of Runs H5, H10, H20 and H40. The first three are at their end-points, and Run H40 is shown at a time which allows comparison. From top to bottom, the cloud’s tangential velocity v_y was 5, 10, 20, and 40 km s^{-1} . The most direct cloud-BH interaction, with $v_y = 5 \text{ km s}^{-1}$, possessed the greatest spread in angular momentum. As v_y increased, the spread in angular momentum shrank, and the flow consolidated to form a single disc, as seen in the $v_y = 20 \text{ km s}^{-1}$ case. When the tangential velocity was 40 km s^{-1} , only a very small portion of the cloud was captured.

earlier numerical experiments (Nayakshin et al. 2007; Bonnell & Rice 2008; Hobbs & Nayakshin 2009; Alig et al. 2011; Mapelli et al. 2012). The masses, semi-major axes and eccentricities of the sinks we discuss in this section are shown in Figure 11.

By the end of Run A at $t = 28300 \text{ yrs}$, nine sinks had formed in the disc and followed orbits with semi-major axes $a \approx 0.095 \text{ pc}$ and eccentricities $e \approx 0.74$. Forming shortly before the simula-

tion’s end, they did not have enough time to accrete to high masses and ranged from one to three M_\odot . While the number of sinks formed in this simulation is well below the observed number of more than a hundred, it is likely that that number would have increased. In the integration step during which the simulation ended, eighteen further sinks were created, more than doubling the total; the step was only half completed. Indeed the rate of sink formation

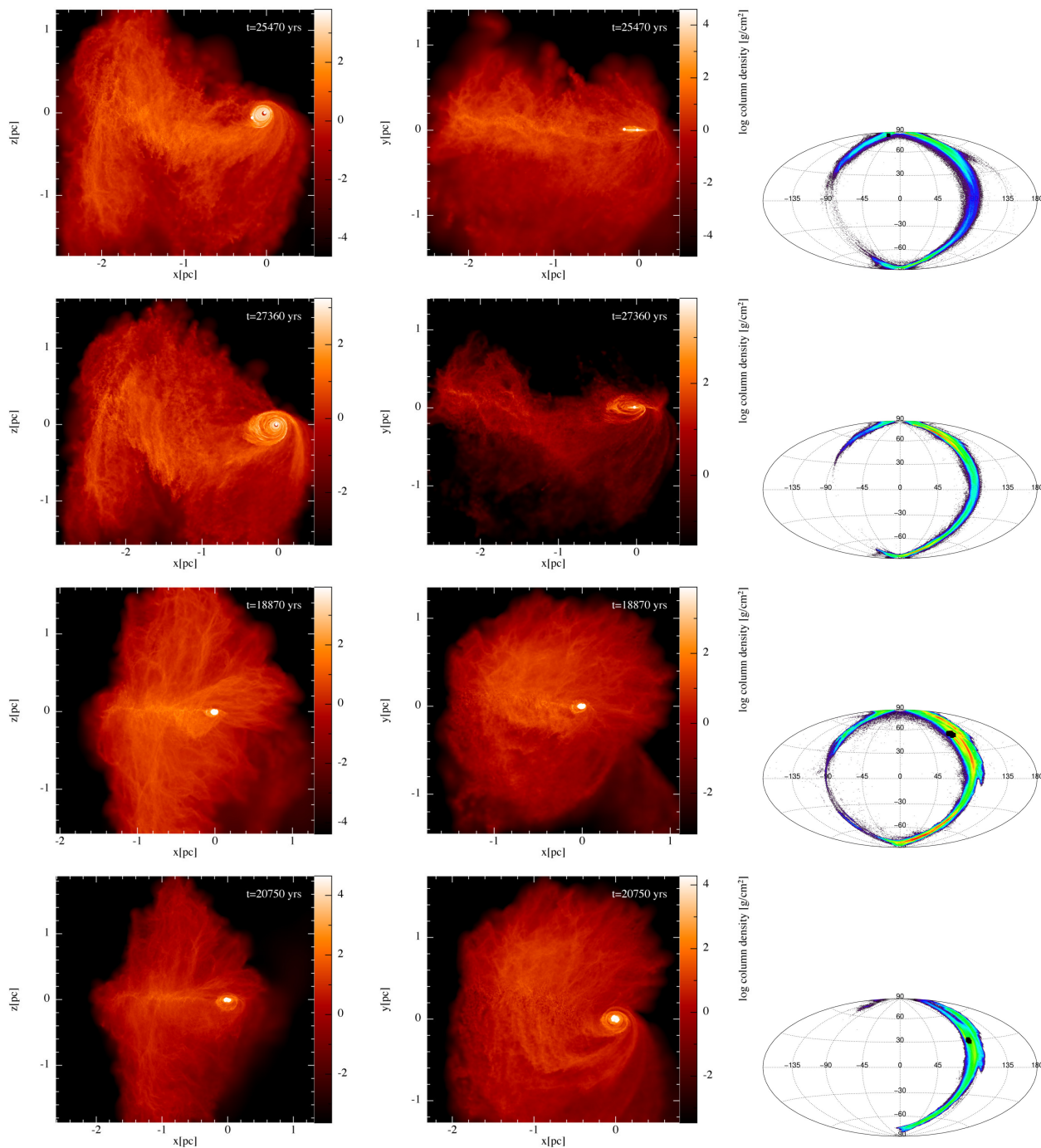


Figure 9. The end states of Runs I5 to I40 are shown here, with one simulation per row. As in Figure 8, the first plot on each row shows column densities in the xz -plane, the second in the xy -plane, and the final shows the spread in the orientation of the particles' angular momenta on the sky. As the initial tangential velocity v_y increased, it can be seen that the primary disc which formed rotated farther into the xy -plane, as was seen with Runs H5 to H40. Runs I20 and I40 were unable to progress as far, and so do not contrast so well with the first two runs. The increased cloud size has broadened the band of angular momentum orientations seen in the third column. Again, increasing v_y has led to the gas motions around the BH growing more aligned, though the enlarged cloud has noticeably helped to preserve the large angular spread of angular momentum when compared to Runs H5 to H40.

was accelerating. Thus our sinks are individually realistic, but our sample incomplete.

The runs using the cloud with mass $M_{\text{cl}} = 10^5 M_{\odot}$ (F and the I runs) were able to form a greater number of sinks. By Run F's end at $t = 25000$ yrs, sixty-four sinks were orbiting the BH. These could be split into two groups separated by semi-major axis. The

first, consisting of fifty-four sinks, had semi-major axes of $a \approx 0.03$ pc and eccentricities $e \approx 0.33$. These began to form at $t = 22070$ yrs. The second population, consisting of ten sinks, began to form at 24520 yrs and had $a \approx 0.07$ pc and $e \approx 0.43$. The mass function of the sinks at the simulation's end are shown in Figure 12.

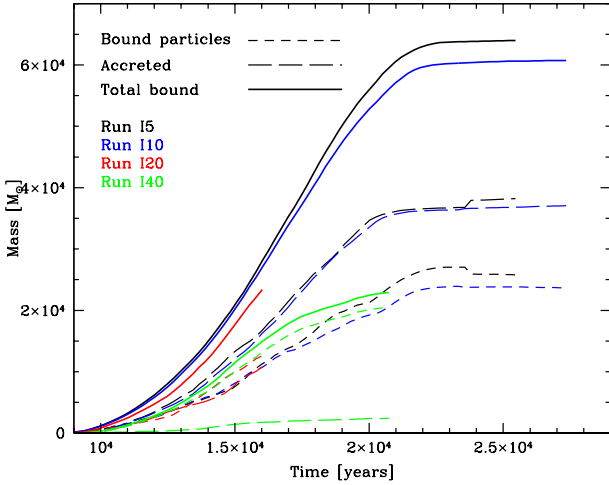


Figure 10. Mass of gas bound to within a distance of 1 pc from the BH (short dashes) and the mass accreted to the BH (long dashes) have been plotted here against time for the I-simulations. The thick solid lines show the sum of the two – this is the total mass bound to within 1 pc. The total mass dropped from $6.4 \times 10^4 M_\odot$ to $2.2 \times 10^4 M_\odot$ as the initial tangential velocity v_y increased from 5 to 40 km s^{-1} . The majority of this is due to a decrease in mass accreted to the BH sink particle. The kinks seen in the 15 lines (black) at 24000 yrs came about as at that time very short timestep gas particles close to the BH were forcibly accreted to it in order for it to run slightly longer. By the end of Runs I5 and I10, roughly twice as much material was accreted to the BH sink as remained bound in the gas phase. In both cases the high infall speed (reducing structure formation time) and low v_y (reducing z -component angular momentum) brought about extremely effective shocking behind the BH, allowing rapid accretion of low angular momentum material.

The sinks were able to accrete quickly; by this point at the end the most massive sink had $55.8 M_\odot$, and the mean mass was $11.6 M_\odot$.

The sinks’ semi-major axes and eccentricities are consistent with those observed, though the former lie at the lower end of the reported range. In this run, the higher gas mass produced greater torques and shocks which were more effective in reducing the angular momentum of the captured material. Thus the gas disc and stellar orbits were smaller and more circular than those seen in Run A.

No sinks formed in misaligned streamers in simulations with slow infall $v_x = -41.5 \text{ km s}^{-1}$. We performed a re-run of Run I10, where a streamer was formed at 17° to the BH accretion disc. Here we allowed the BH to accrete all material within 0.02 pc without test and sinks to form with ratio of thermal to gravitational energy of one, as opposed to 0.5 which is otherwise used. With these changes the simulation could run to $t = 31130$ yrs, and the misaligned streamer was able to become dense enough that a second population of sinks formed 17° from the first. The simulation at its end is shown in Figure 13.

The fifty-two sinks in the first population had semi-major axes of $\approx 0.2 \text{ pc}$ and eccentricities of ≈ 0.4 ; the fifteen in the second population, formed in the streamer, had semi-major axes of $\approx 0.3 \text{ pc}$ and eccentricities of ≈ 0.45 . Mass functions are shown in Figure 14. While the outer misaligned sinks are at lower masses, both populations contain sinks which have been allowed to accrete to high masses.

The MFs shown (Figures 12 for Run F and 14 for the re-run of I10) do not resemble a standard Salpeter (1955) IMF, being flat in

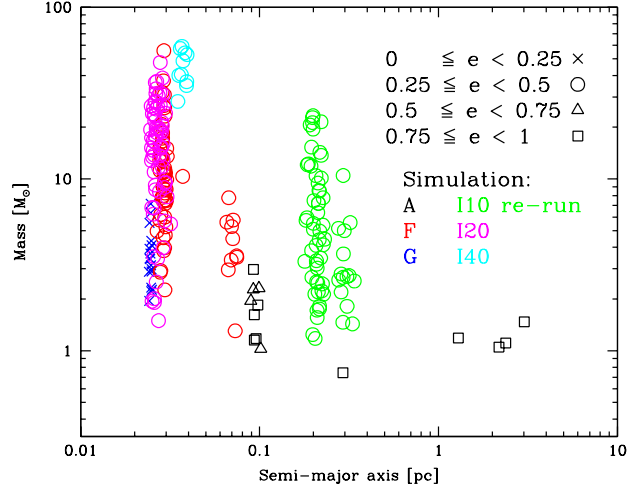


Figure 11. The masses of sinks from several simulations are plotted against their semi-major axes. The symbols’ colours show which run they were from, and the shape indicates which eccentricity range that sink inhabited. Most simulations’ sinks are seen to inhabit well-defined regions. The lowest eccentricity sinks were only found at the lower end of the semi-major axis range as a direct result of the cancellation of angular momentum by gas during shocking and torquing. The highest mass sinks were also found at low semi-major axes. Higher eccentricity sinks orbited at larger distances, and had lower masses. The inner and outer populations of sinks in Run F and the re-run of I10 (where the outer was 17° out-of-plane from the inner) can be clearly distinguished. Those in Run A at the largest distances were formed during infall and did not belong to the disc. Perhaps most noticeably, eccentricities in the range of 0.25 to 0.5 were by far the most common, and covered almost the complete range of masses and semi-major axes.

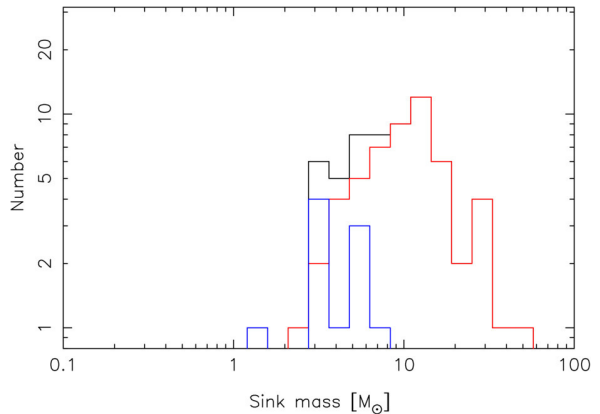


Figure 12. Mass functions for the two populations of sinks seen at 25000 yrs in Run F. The red line shows the mass function for all sinks with semi-major axes $a \leq 0.05 \text{ pc}$, and the blue line those with $a > 0.05 \text{ pc}$. The black line shows the total. While both populations contain sinks which would be considered high mass, those in the outer population have had less time to accrete and so do not reach the extremely high masses of those in the inner population. No masses are below $\sim 0.9 M_\odot$, equivalent to 30 gas particles.

logspace from one to ten M_\odot . The number of sinks in each bin for Run F’s inner population actually increases, peaking in the range of tens of solar masses before falling again. The observed IMF is likewise weighted towards the higher end (Bartko et al. 2010), apparently a violation of a ‘global’ Salpeter-like IMF. Simulations suggest this is due to high gas temperatures and preferential for-

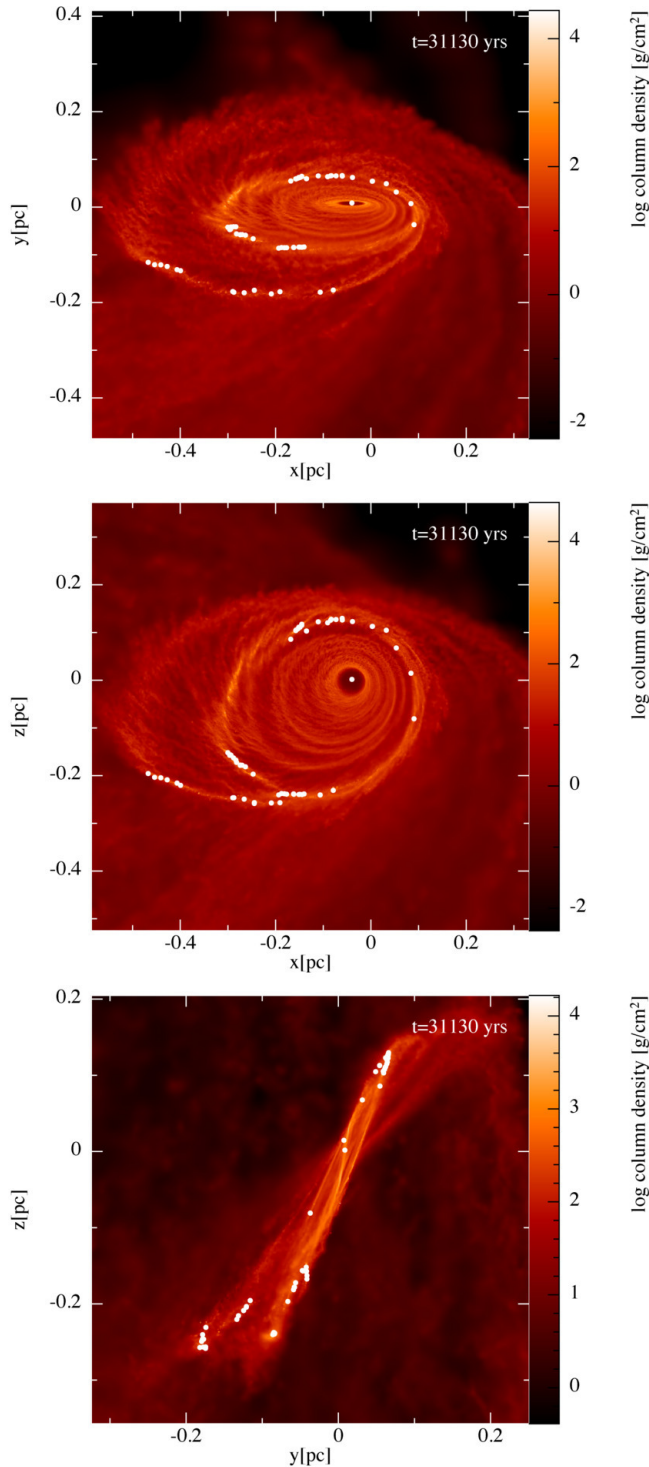


Figure 13. Column densities for the re-run of I10 in the xy , xz and yz planes at the simulation’s end at $t = 31130$ yrs. By this point the disc and gas streamers feeding it had grown dense enough that sink formation was underway. The streamers were oriented 17° out-of-plane from the disc, resulting in two stellar systems separated by this angle.

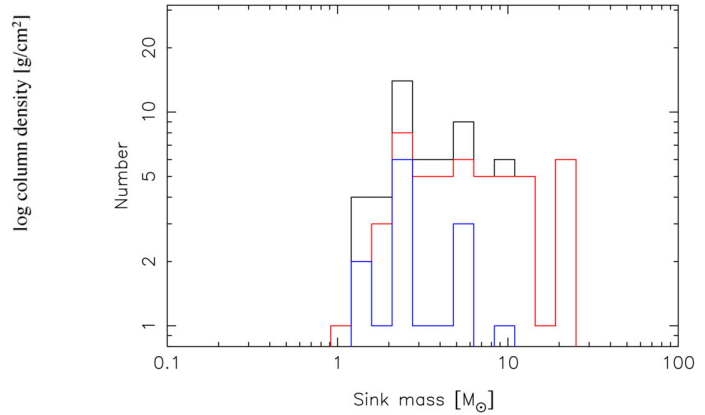


Figure 14. Mass function for the re-run of I10 at $t = 31130$ yrs. The red and blue lines represent the individual mass functions for the disc ($a \approx 0.2$ pc) sinks and the streamer ($a \approx 0.3$ pc) sinks, respectively. The underlying black line shows the MF for the total population. The outer population, which formed later on, consists of lower mass sinks, while the inner population formed earlier and so had time to accrete to the high masses we see here.

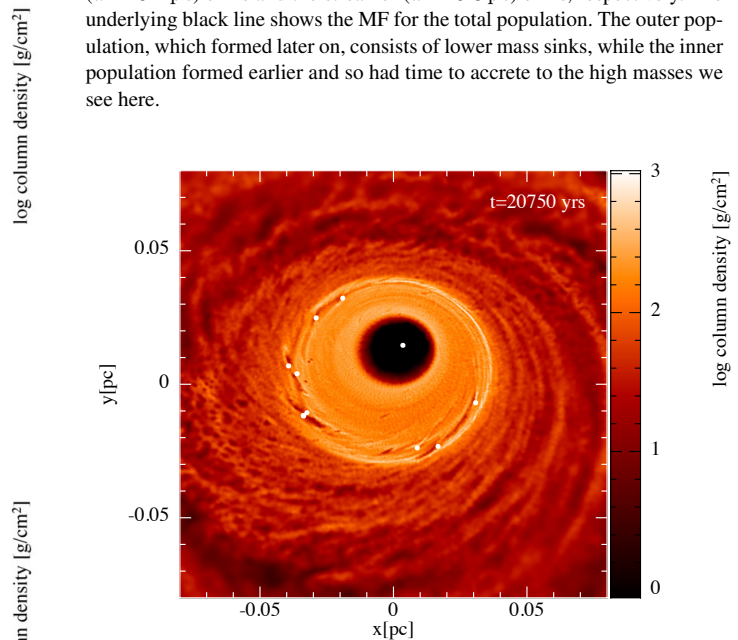


Figure 15. Column density in the xy -plane for Run I40 at its end-time of 20750 yrs. White dots show the locations of sink particles. The high initial tangential velocity of 40 km s^{-1} has suppressed the formation of any misaligned gas flows. Shocked gas has formed a small, low-eccentricity disc. The ten sinks within it have $a \approx 0.037$ pc and $e \approx 0.3$. Gaps in the disc mark the regions where the sinks have been accreting from the gas, raising them to several tens of solar masses within 5000 yrs.

mation of high-mass fragments due to tidal forces (Bonnell & Rice 2008). Variable tidal forces experienced throughout an eccentric disc such as those in our simulations were also found by Alexander et al. (2008) to increase the fragment mass when compared to those in circular discs. It is important to emphasise that our plots are not a numerically-derived initial mass function, as the sinks are still accreting. This does however show that that our sinks have been able to grow to tens of solar masses within only a few thousand years.

The gaseous discs which formed within Run I20 and I40 were also able to form a substantial number of sinks. Considerable shocking had taken place within the gas, and so the disc and stellar orbits were small with semi-major axes $a \approx 0.027$ pc and eccentricities $e \approx 0.4$. The mass function resembled that of the inner population of Run F (red line, Figure 12), but it was actually shifted

even further towards high masses, peaking at $\sim 30M_{\odot}$. Run 140 formed only ten sink particles (see Figure 15), with $a \approx 0.037$ pc and $e \approx 0.3$. Despite their small number, their masses were very large – the lowest sink mass was $28M_{\odot}$, and the highest $59M_{\odot}$. Noticeable openings in the disc show the regions from which they had been accreting.

4.3 Subsequent star formation

By the time our simulations ended, no sink particles had been created in streamers at an angle beyond 17° from the principle gas disc. Our simulations were only able to run for a few tens of thousands of years. Given the physical conditions at the end of the simulations we expect further fragmentation to occur.

Gammie (2001) found that only gas which is able to cool over a timescale t_{cool} shorter than three times the dynamical timescale t_{dyn} may fragment – see also Rice et al. (2003) and Rice, Lodato & Armitage (2005)). Figure 16 shows the cooling and dynamical timescales for Run A at its end ($t = 28300$ yrs). A wide dispersion of t_{cool} over several orders of magnitude above and below the critical $t_{\text{cool}} = 3t_{\text{dyn}}$ line can be seen throughout. Within $a \approx 0.1$ pc, the majority of the gas had t_{cool} between ~ 100 and $\sim 10^4$ yrs. This gas should be able to cool sufficiently to form additional sinks.

That gas for which the density exceeded the tidal value is also marked in Figure 16. Of the $17904M_{\odot}$ of gas which had not been accreted to the BH or formed sink particles, $7353M_{\odot}$ had $t_{\text{cool}} \leq 3t_{\text{dyn}}$; of that, $1689M_{\odot}$ exceeded the tidal density. This self-gravitating gas with a short cooling time may fragment and collapse. If we then assume that all this gas was destined to form stars, it suggests a final star formation efficiency of 8.5 per cent for the initial cloud of $2 \times 10^4 M_{\odot}$.

We can also estimate the properties of the stars which will form. We take all the gas from Figure 16 that has a short enough t_{cool} for collapse and plot the Jeans mass against semi-major axis; this can be seen as the first plot in Figure 17. Again we highlight those particles exceeding the tidal density. We also calculate the angle between the y -axis and the projected yz -angular momentum for this gas; this is shown in the second plot of Figure 17. The gas on smaller orbits has Jeans masses varying from 0.1 to $300M_{\odot}$. The second plot shows that this gas also covers about 50° in orbital inclination, centred roughly around $\theta \approx 90^{\circ}$ i.e. angular momentum vector aligned with the z -axis. This reflects that by the simulation's end some gas was still in the process of settling into the disc plane.

The gas on larger orbits can be seen in second plot of Figure 17 to be restricted to an orbital orientation of $\theta \approx 40^{\circ}$ – this is the misaligned streamer. While it seems that stars should form here over time, the Jeans masses indicated previously for this gas are much lower, ranging from 0.5 to $2M_{\odot}$. Also, the semi-major axis for streamer gas extends to distances of 10 pc. The mass of gas in the streamer which may form stars is very low however, at only $21M_{\odot}$.

5 CONCLUSIONS

Recent observations indicate the presence of two misaligned discs of massive stars around Sagittarius A* (Paumard et al. 2006; Bartko et al. 2009). These stars all formed at roughly the same time, somewhere between 6 and 10 million years ago. If these stars were formed via *in situ* disc fragmentation (Levin & Beloborodov 2003), two misaligned discs or streamers are required. In this paper we

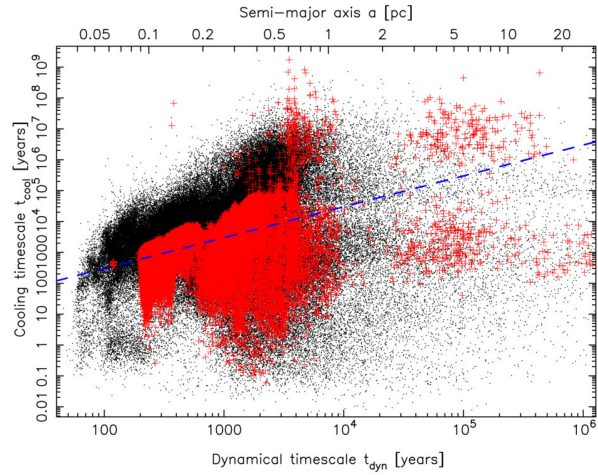


Figure 16. Cooling and dynamical timescales (with corresponding semi-major axis) for all particles in Run A at $t = 28300$ yrs. Those marked with red crosses are above the tidal density; the dashed line marks $t_{\text{cool}} = 3t_{\text{dyn}}$. Gas below this line can fragment according to Gammie (2001).

have examined whether the infall of a single cloud to the BH to provide the star formation material is a plausible scenario.

the cloud need also have an impact parameter which is smaller than the largest extent of the cloud. In addition, significant sub structure need exist within the cloud, such as produced here by turbulence, to avoid symmetric shocks behind the black hole. This ensures sufficient angular momentum remains in the bound gas to form massive gaseous discs around the hole.

We ran smoothed particle hydrodynamics (SPH) simulations of the infall of several clouds towards a $4 \times 10^6 M_{\odot}$ black hole (BH). Crucially, the cloud was given an ellipsoidal geometry, with its major axis oriented perpendicular to its orbital plane. The cloud's orbit was highly radial to the point that the cloud marginally engulfed the BH. The combination of the two spread the distribution of gas particles' angular momenta about the BH over a large region of the sky. When the cloud reached the BH, its central regions were tidally sheared and captured to form a disc. The extremities flowed around the BH at large angles to one another and to the disc. If the cloud were to have uniform density, these flows would meet at the midplane and shock to remove their out-of-plane motion – this is essentially the mechanism of Wardle & Yusef-Zadeh (2008) which allows the construction of small accretion discs. The cloud's impact parameter was also required to be smaller than the largest extent of the cloud to ensure a sufficient spread in angular momentum. In addition, significant sub-structure was needed within the cloud, such as that produced here by turbulence, to avoid symmetric shocks behind the BH. This ensures sufficient angular momentum remains in the bound gas to form massive gaseous discs around the hole. These requirements indicate that the parameter space allowing the formation of a misaligned disc or streamer is somewhat limited.

We also tested high infall speeds using -150 km s^{-1} while varying the tangential speed from 5 km s^{-1} to 40 km s^{-1} . The faster infall led to less structure forming by the time the cloud reached the BH. As angular momentum was modified with the tangential speed, we observed the gas flows rotating with increasing v_y . In Run I10, which used a $10^5 M_{\odot}$ cloud with $v_y = 10 \text{ km s}^{-1}$, a streamer was able to form, though it was only misaligned from the primary disc by 17° . In a re-run it was however able to progress

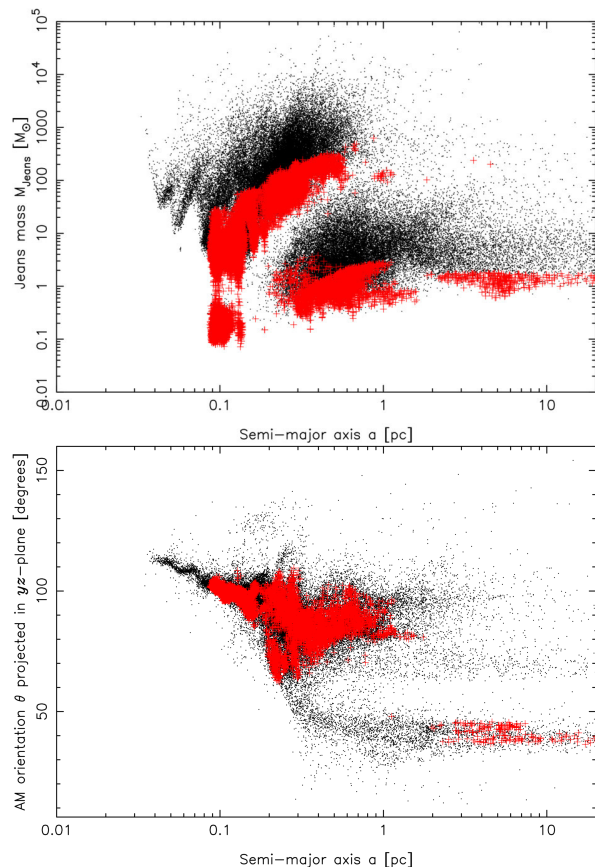


Figure 17. Here we compare both the Jeans mass M_{Jeans} and orbital inclination θ with the semi-major axis a of gas in Run A at $t = 28300$ yrs. Here we define the orbital inclination to be $\theta = \tan(l_z/l_y)$ i.e. the angle between the simulation y -axis and the projection of the angular momentum vector into the yz -plane. Since the x -component of the angular momentum is small (Figure 4), $\theta = 0^\circ$ means the gas is orbiting almost in the xz -plane, and 90° in the xy -plane. We only plot that gas which fulfilled the Gammie criterion for fragmentation in Figure 16, that is to say lay beneath the line. Red crosses again mark gas denser than the local tidal value. The gas in the disc follows orbits with $a \lesssim 1$ pc. Jeans masses range from 0.1 to $300M_\odot$. The streamer can be seen in the second plot at $\theta \approx 40^\circ$ and extending to large semi-major axes. The first plot shows that Jeans masses within it are small, reaching at most $2M_\odot$.

far enough that sinks formed within both the central disc and the streamer.

Across the simulations sink eccentricities varied from 0.15 to 0.7; Bartko et al. (2009) reported the clockwise stars (the primary structure) to have a mean eccentricity of 0.35. Semi-major axes of both the gas discs and any sink particles which formed within them were small. While some runs' discs were as large as 0.3 pc, it was not uncommon for them to be smaller than 0.1 pc. Meanwhile studies on the stellar discs has found them to inhabit a region between 0.05 and 0.5 pc, or $1 - 10''$ (eg. Genzel et al. 2003; Paumard et al. 2006; Lu et al. 2009; Bartko et al. 2009).

In Run A, Jeans masses for gas above the tidal density in the inner disc ranged up to $\sim 100M_\odot$. Streamer material orbited with semi-major axes of up to 10 pc. Only $21M_\odot$ of gas within the streamer exceeded both the tidal density and was capable of fragmentation (Gammie 2001). Jeans masses were much lower, between 0.5 and $2M_\odot$. As well as being separated from the main disc by 60° , the gas capable of forming stars was only found on orbits

with semi-major axes greater than 1 pc. In this instance, it seems unlikely that a misaligned disc such as that observed will come about, but it could allow for the simultaneous formation of disc stars and additions to any present nuclear cluster. Given the sensitivity to initial conditions that we found, it is not impossible that another cloud would have formed stars on orbits similar to those observed. The other runs were capable of fragmentation with similar Jeans masses, but did not display the presence of the streamer.

Depending on the cloud structure and orbit a variety of end configurations seem achievable and may provide a route to, for example, the counter-rotating gas discs of Nixon, King & Price (2012). We know from previous work that the formation of large numbers of stars via fragmentation is viable (Nayakshin et al. 2007; Bonnell & Rice 2008; Hobbs & Nayakshin 2009; Alig et al. 2011; Mapelli et al. 2012). Together these indicate that a single gas cloud should be able to provide all the material for forming multiple stellar discs. However, the requirements placed on the cloud's shape, structure and orbit as stated above may limit the effectiveness of the method.

ACKNOWLEDGEMENTS

WEL's PhD is supported by an STFC studentship from the Government of the United Kingdom. IAB acknowledges funding from the European Research Council for the FP7 ERC advanced grant project ECOGAL. WKMR acknowledges support from STFC grant ST/J001422/1. This work was supported by the Swedish Research Council (grants 2008–4089 and 2011–3991). The simulations presented here were run on UKMHD's Wardlaw cluster at St Andrews. Rainer Schödel provided excellent advice regarding the nuclear stellar cluster which we used to model its potential and for which we greatly thank him. Our column density plots were produced using Daniel Price's SPLASH software (Price 2007). Finally, thanks go to the anonymous referee who provided many useful comments, allowing the paper to be improved.

REFERENCES

- Alexander, T., 2005, PhR, 419, 65
- Alexander R.D., Armitage P.J., Cuadra J., Begelman M.C., 2008, ApJ, 674, 927
- Alig C., Burkert A., Johansson P.H., Schartmann M., 2011, MNRAS, 412, 469
- Bartko H. et al., 2009, ApJ, 697, 1741
- Bartko H. et al., 2010, ApJ, 708, 834
- Bate M.R., Bonnell I.A., Price N.M., 1995, MNRAS, 227, 362
- Benz W., 1990, in Buchler J.R., ed., Proceedings of the NATO Advanced Research Workshop on The Numerical Modeling of Nonlinear Stellar Pulsations: Problems and Prospects, Kluwer, Dordrecht, p. 269
- Benz W., Bowers R.I., Cameron, A.G.W., Press, R.L., 1990, ApJ, 348, 647
- Bonnell I.A., Rice W.K.M., 2008, Science, 321, 1060
- Buchholz R.M., Schödel R., Eckart A., 2009, A&A, 499, 483
- Christopher M.H., Scoville N.Z., Stolovy S.R., Yun M.S., 2005, ApJ, 622, 346
- Collin S., Zahn J.-P., 1999, A&A, 344, 433
- Dobbs C.L., Bonnell I.A., Clark P.C., 2005, MNRAS, 360, 2
- Dubinski J., Narayan R., Phillips T.G., 1995, ApJ, 448, 226

- Forgan D., Rice K., Stamatellos D., Whitworth A., 2009, MNRAS, 394, 882
- Gammie C.F., 2001, ApJ, 553, 174
- Genzel R., Thatte N., Krabbe A., Kroker H., Tacconi-Garman L.E., 1996, ApJ, 472, 153
- Genzel R., et al., 2003, ApJ, 594, 812
- Genzel R., Eisenhauer F., Gillessen S., 2010, Rev. Mod. Phys., 82, 3121
- Gerhard O., 2001, ApJ, 546, L39
- Ghez A.M., et al., 2008, ApJ, 689, 1044
- Goodman J., 2003, MNRAS, 339, 937
- Hansen B.M.S., Milosavljević M., 2003, ApJL, 593, 77
- Hernquist L., Katz, N., 1989, ApJSS, 70, 419
- Hobbs A., Nayakshin S., 2009, MNRAS, 394, 191
- Jackson J.M., Geis N., Genzel R., Harris A.I., Madden S., Poglitsch A., Stacey G.J., Townes C.H., 1993, ApJ, 402, 173
- Kolykhalov P.I., Syunyaev R.A., 1980, SvAL, 6, 357
- Krabbe A., et al., 1991, ApJ, 382, L19
- Krabbe A., et al., 1995, ApJ, 447, L95
- Levin Y., Beloborodov A.M., 2003, ApJ, 590, L33
- Levin Y., 2007, MNRAS, 374, 515
- Lu J.R., Ghez A.M., Hornstein S.D., Morris M.R., Becklin E.E., Matthews K., 2009, ApJ, 690, 1463
- Mapelli M., Hayfield T., Mayer L., Wadsley J., 2012, ApJ, 749, 168
- Martín-Pintado J., de Vicente P., Fuente A., Planesas P., 1997, ApJL, 482, 45
- Mayer L., Lufkin G., Quinn T., Wadsley J., 2007, MNRAS, 661, L77
- Merritt D., 2010, ApJ, 718, 739
- Monaghan J.J., 1992, ARA&A, 30, 543
- Nayakshin S., Cuadra J., 2005, A&A, 437, 437
- Nayakshin S., Cuadra J., Springel V., 2007, MNRAS, 379, 21
- Nixon C.J., King A.R., Price D.J., 2012, MNRAS, 422, 2547
- Paumard T. et al., 2006, ApJ, 643 1011
- Price D.J., 2007, PASA, 24, 159
- Rice W.K.M., Armitage P.J., Bate M.R., Bonnell I.A., 2003, MNRAS, 339, 1025
- Rice W.K.M., Lodato G., Armitage P.J., 2005, MNRAS, 364, L56
- Salpeter E.E., 1955, ApJ, 121, 161
- Schödel R., et al., 2007, A&A, 469, 125
- Schödel R., Merritt D., Eckart A., 2009, A&A, 502, 91
- Shlosman I., Begelman M.C., 1989, ApJ, 341, 685
- Stamatellos D., Whitworth A.P., Bisbas T., Goodwin S., 2007, A&A, 475, 37
- Toomre A., 1964, ApJ, 139, 1217
- Tsuboi M., Tadaki K.-I., Miyazaki A., Handa T., 2011, PASJ, 63, 763
- Wardle M., Yusef-Zadeh F., 2008, ApJL, 683, 37